Structural analysis of xylanase inhibitor protein I (XIP-I), a proteinaceous xylanase inhibitor from wheat (*Triticum aestivum*, var. Soisson)

Françoise PAYAN*[1], Ruth FLATMAN†, Sophie PORCIERO*, Gary WILLIAMSON†[2], Nathalie JUGE†‡ and Alain ROUSSEL*

*Architecture et Fonction des Macromolécules Biologiques, UMR6098, CNRS and Universities Aix-Marseille I and II, 31 chemin Joseph Aiguier, F-13402 Marseille, France, †Institute of Food Research (IFR), Colney Lane, Norwich NR4 7UA, U.K., and ‡Institut Méditerranéen de Recherche en Nutrition, UMR INRA 1111, Faculté des Sciences et Techniques de St Jérôme, avenue Escadrille Normandie Niemen, F-13397 Marseille, France

A novel class of proteinaceous inhibitors exhibiting specificity towards microbial xylanases has recently been discovered in cereals. The three-dimensional structure of xylanase inhibitor protein I (XIP-I) from wheat (*Triticum aestivum*, var. Soisson) was determined by X-ray crystallography at 1.8 Å (1 Å = 0.1 nm) resolution. The inhibitor possesses a $(\beta/\alpha)_8$ barrel fold and has structural features typical of glycoside hydrolase family 18, namely two consensus regions, approximately corresponding to the third and fourth barrel strands, and two non-proline *cis*-peptide bonds, Ser[36]–Phe and Trp[256]–Asp (in XIP-I numbering). However, detailed structural analysis of XIP-I revealed several differences in the region homologous with the active site of chitinases. The catalytic glutamic acid residue of family 18 chitinases [Glu[127] in hevamine, a chitinase/lysozyme from the rubber tree (*Hevea brasiliensis*)] is conserved in the structure of the inhibitor (Glu[128]), but its side chain is fully engaged in salt bridges with two neighbouring arginine residues. Gly[81], located in subsite −1 of hevamine, where the reaction intermediate is formed, is replaced by Tyr[80] in XIP-I. The tyrosine side chain fills the subsite area and makes a strong hydrogen bond with the side chain of Glu[190] located at the opposite side of the cleft, preventing access of the substrate to the catalytic glutamic acid. The structural differences in the inhibitor cleft structure probably account for the lack of activity of XIP-I towards chitin.

Key words: family 18 chitinase, hevamine, wheat, X-ray structure, xylanase inhibitor.

INTRODUCTION

Plants contain a wide range of enzymes which hydrolyse complex carbohydrate polymers. These endogenous enzymes are often regulated by proteinaceous inhibitors that may also play an important role in plant defence by preventing enzymic hydrolysis by micro-organisms and predators. A novel class of endoxylanase inhibitors has been discovered in cereals [1,2] for which no structural data are available. The endo-1,4-β-D-xylanases (EC 3.2.1.8) produced by some bacteria, fungi and plants, hydrolyse the β-(1,4) glycosidic linkages in the xylan component of plant cell walls. On the basis of amino acid sequence similarities, xylanases have been classified into family-10 (GH-10) and family-11 (GH-11) glycoside hydrolases (GHs) [3]. Family GH-10 enzymes are $(\beta/\alpha)_8$ barrels with the two catalytic residues located at the C-termini of strands β-4 and β-7 [4], whereas family GH-11 enzymes are β-jelly-roll enzymes in which the substrate-binding groove is formed by the concave face of one of the β-sheets [5]. Although the catalytic action of xylanases is reasonably well understood, only little information is available on the mechanism underlying their inhibition by naturally occurring inhibitors. Two types of xylanase inhibitor with different specificities have been purified to date from wheat (*Triticum aestivum* var. Soisson). TAXI (*T. aestivum* xylanase inhibitor) is a high-pI, non-glycosylated protein with a molecular mass of approx. 40 kDa [2]. At least two inhibitors of this type (TAXI-I and TAXI-II) with different pI values (8.8 and ≈9.3 respectively) and various specificities towards different endoxylanases have been identified [6]. Xylanase inhibitor protein I (XIP-I) is a glycosylated monomeric protein with a molecular mass of 29 kDa and pI values of 8.7–8.9 [1]. It inhibits fungal xylanases from both family-10 and -11 [7,8], apart from the family GH-10 *Aspergillus aculeatus* xylanase, with K_i values ranging from 3.4 to 610 nM, but does not inhibit bacterial family-10 and -11 xylanases [7]. The kinetics of inhibition are competitive and reversible [1,7,8].

On the basis of amino acid sequence similarity, XIP-I [9] is a member of the GH family 18 [http://afmb.cnrs-mrs.fr/CAZy/index.html; the CAZy database describes the families of structurally related catalytic and carbohydrate-binding modules (or functional domains) of enzymes that degrade, modify or create glycosidic bonds]. Among the plant members of family-18 chitinases, the three-dimensional structures of hevamine, a chitinase/lysozyme isolated from the rubber plant (*Hevea brasiliensis*) [10], concanavalin B from *Canavalia ensiformis* (jack-bean) [11] and narbonin from *Vicia narbonensis* (Narbonne vetch) [12] have been determined. They all show the $(\beta/\alpha)_8$ barrel fold and the two consensus regions characteristic of the GH family 18 [10,11]. XIP-I shows 47, 42 and 30 % similarity and 36, 33 and 14 % identity with hevamine [13], concanavalin B [14] and narbonin [15] sequences respectively. Hevamine exhibits both lysozyme and chitinase activity [16], whereas concanavalin B and narbonin [11,12], as also reported for XIP-I [1,7], do not show any chitinase activity.

Biochemical characterization of the interaction between a GH-11 xylanase from *Aspergillus niger* and XIP-I was recently carried out using site-directed mutagenesis [17]. The *A. niger* xylanase molecule has been compared with the shape of the right hand with the 'fingers' at the top, the 'palm' at the bottom and the thumb on the right hand side of the molecule [18]. Mutation of Asn[117], located at the end of the β-bend occurring at the tip of the thumb, led to the abolition of the interaction between XIP-I and the mutant enzyme. The general shape of the 'thumb' is conserved

Abbreviations used: GH, glycoside hydrolase; r.m.s. root mean square; tri-NAG, *N*,*N*′,*N*″-triacetylchitotriose; XIP-I, xylanase inhibitor protein I.

[1] To whom correspondence should be addressed (fran@afmb.cnrs-mrs.fr).
[2] Present address: Nestlé Research Centre, Vers-Chez-Les-Blanc, PO Box 44, CH-1000 Lausanne 26, Switzerland.

in all the other family-11 xylanases, and the 'thumb' hairpin loop of family-11 xylanases was therefore suggested to be the XIP-I-binding site [17]. Here we present the first three-dimensional structure of a plant xylanase inhibitor and discuss the reasons for the lack of chitinase activity observed for this member of the GH family 18.

MATERIALS AND METHODS

Purification of the xylanase inhibitor

The xylanase inhibitor was purified from wheat (*T. aestivum* var. Soisson) flour as described previously [1].

Crystallization and data collection

XIP-I crystals were obtained by vapour diffusion in hanging drops at 20 °C. The protein solution used in the crystallization procedure contained 3.6 mg/ml protein in 50 mM Mes, pH 5.5. The hanging drops consisted of 1 μl of XIP-I solution together with 1 μl of the reservoir solution composed of 0.1 M Tris/HCl, pH 8.5, with 28 % PEG 4000 [poly(ethylene glycol) of molecular mass 4000] and 0.2 M LiCl. Crystals with a maximum size of 0.15 mm × 0.15 mm × 0.5 mm grew within 10 days. These crystals, which belonged to the $P4_32_12$ space group, had the following cell dimensions: $a = b = 58.5$ Å, $c = 193.7$ Å and diffracted to 1.8 Å resolution (1 Å = 0.1 nm). Ethylene glycol was used at a concentration of 30 % as the cryoprotectant in the following data-collection stage.

X-ray diffraction data were collected at 100 K on an ADSC Q4 CCD (charge-coupled-device) detector using synchrotron radiation at ID14-EH2 beamline in the European Synchrotron Radiation Facility (Grenoble, France). Data processing was performed using the DENZO and SCALEPACK programs [19]. Data collection statistics are given in Table 1.

Structure determination and refinement

The structure of XIP-I was solved by molecular replacement using the AMoRe program [20]. The structure of hevamine (pdb code 2HVM) was used as the search model. The rotation function yielded one solution and the translation function a unique solution, with a correlation coefficient and an *R* factor of 28.3 and 50.6 % respectively, with data between 10 and 3 Å.

Refinement procedures were performed using the CNS (Crystallography & NMR System) program [21]. The starting crystallographic *R* factor for the molecular replacement solution was 0.36 with data between 15 and 2.3 Å. After manual corrections of the model using the TURBO-FRODO program [22], interspersed with cycles of slow cooling protocol refinement with all data up to 1.8 Å resolution, a final *R* factor of 0.197 ($R_{free} = 0.22$) was obtained. Water molecules were added and inspected manually. The co-ordinates have been deposited with the Brookhaven Protein Data Bank with accession number 1om0.

RESULTS AND DISCUSSION

Quality of the structure

The sequence of XIP-I from wheat (*T. aestivum* var. Soisson) [9] was used to build the present model. The final structure consisted of all 274 amino acid residues of the sequence. All the residues have conformational angles in permitted regions of the Ramachandran plot [23], and none of these are located in 'generously allowed' regions as defined by PROCHECK [24]. The final ($2F_o-F_c$) electron-density map (1 σ contoured) showed that all residues of the model were well fitted. A long loop protruding in the solvent (residues 147–153) is characterized by temperature-factor values higher than the average B value. However, the loop was well defined by the electron density; Arg^{149} emerging from the the bulky head of this loop region is fully defined in the electron density. In the crystal packing the facing residue, His^{129}, is observed in alternative conformation. Further structure quality indicators are given in Table 1. The presence of glycosylation on purified XIP-I has been previously reported [1], and the determined structure allowed identification of two N-glycosylation sites at Asn^{89} and Asn^{265}. In both cases an *N*-acetylglucosamine entity N-linked to the amide nitrogen atom in the side chain of an asparagine could be accommodated into the electron-density pattern. A total of 297 ordered water molecules were identified. Some electron-density regions corresponding to ethylene glycol molecules originating from the cryoprotectant were visible, and these molecules were added to the model.

Table 1 Data collection (a) and final refinement (b) statistics

(a)

Data collection parameter	Value
Resolution limit (Å)	20–1.8
Completion (%)	99.1 (99.5)
Redundancy	4.7 (4.6)
R_{sym}*	7.4 (24.5)
$I/\sigma(I)$	11.2 (2.3)

(b)

Refinement parameter	Value
Resolution limits (Å)	15–1.8
Number of reflections (test set)	31670 (1573)
Number of protein atoms	2140
Number of sugar atoms	28
Number of cryoprotectant atoms	36
Number of water molecules	297
Final R_{factor}†/R_{free}‡ (%)	19.7 / 22.5
B factors (Å^2)	
Protein	25.4
Sugar	55.0
Cryoprotectant	47.6
Water molecules	43.2
Root mean square deviations	
Bond (Å)	0.0063
Angles (°)	1.34
Improper/dihedral angles (°)	0.68/23.9

* $R_{sym} = \Sigma_h \Sigma_i |I_{hi} - \langle I_h \rangle| / \Sigma_h \Sigma_i I_{hi}$

† $R_{factor} = \Sigma_h ||F_{obs}| - |F_{calc}|| / \Sigma_h |F_{obs}|$, where F_{obs} and F_{calc} are the observed and calculated structure factor amplitudes respectively.

‡ R_{free} is calculated with 5 % of the diffraction data, which were not used during the refinement.

Overall three-dimensional structure of XIP-I

The architecture of XIP-I consists of a single elliptical $(\beta/\alpha)_8$ scaffold, the top of which is decorated by loops arranged to form a long depression running along one face of the molecule. The nomenclature of the α-helices and β-strands is illustrated in Figure 1, and the loops surrounding the depression are labelled (Figure 1B). The connecting loops between the C-terminus of a strand and the N-terminus of a helix will hereafter be referred to as '$L\beta_x\alpha_x$'; they are of variable length, ranging from 6 to 18 residues. In addition to the loops $L\beta_x\alpha_x$ at the C-termini of the β-barrel strands, the long loop $L\alpha_4\beta_5$ protrudes in the solvent from

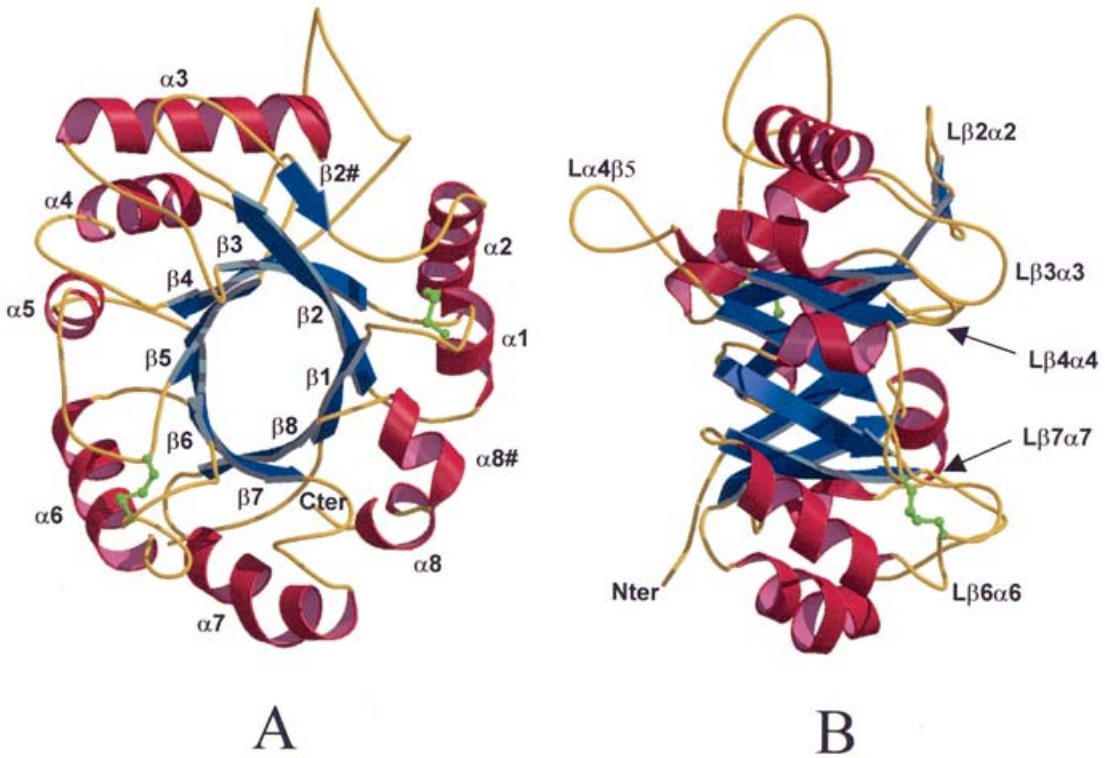

Figure 1 Secondary and tertiary structures of XIP-I

(**A**) Ribbon diagram of XIP-I with the secondary-structural components numbered as in the text; the disulphide bridges are shown (green). The view is down the axis of the eight-stranded β-barrel. (**B**). The molecule is rotated about 90 ° along the vertical axis relative to the orientation of (**A**). The loops ($L\beta_x\alpha_x$) delineating the cleft are labelled. The Figure was drawn with MOLSCRIPT [29].

the opposite face of the molecule and the loop $L\alpha_3\beta_4$ emerges at the extremity of the longest axis of the helliptical architecture (Figure 1B).

Two disulphide bridges are present between residues Cys^{25} and Cys^{66} and between Cys^{164} and Cys^{195}. The Cys^{25}–Cys^{66} bridge connects helices $\alpha1$ and $\alpha2$, whereas Cys^{164}–Cys^{195} connects the loops $L\beta_5\alpha_5$ and $L\beta_6\alpha_6$ (Figure 1).

$L\beta_3\alpha_3$, $L\beta_4\alpha_4$, $L\beta_6\alpha_6$ and $L\beta_7\alpha_7$ define the walls of the depression (Figure 1B), while the flat loops $L\beta_1\alpha_1$, $L\beta_2\alpha_2$ (the end part), together with the opposite loop, $L\beta_5\alpha_5$, constitute the extremities of this groove. This rather flat depression (Figure 2A, right-hand panel) is similar to the substrate-binding cleft observed in the structure of hevamine, a class III chitinase (member of family 18) isolated from the rubber plant *H. brasiliensis*, which exhibits both lysozyme and chitinase activity [10]. In hevamine, the C-terminal residues of the β-barrel strands form the centre of the substrate-binding cleft, whereas $L\beta_7\alpha_7$ and $L\beta_3\alpha_3$ form the walls of the cleft (Figure 2A, left-hand panel). These loops play an essential role in the carbohydrate-recognition process and contribute importantly to the substrate specificity [10,25]. In the structure of XIP-I, the $L\beta_7\alpha_7$ loop (residues 222–232) is moved out toward the solvent, thus broadening the cleft (Figure 2A, right-hand panel), while in hevamine the loop is turned in toward the substrate ligand. Loop $L\beta_3\alpha_3$, forming the opposite side of the cleft, also shows a similar variation, although less pronounced. $L\beta_7\alpha_7$ and $L\beta_3\alpha_3$ bear important residues involved in the architecture of subsite -1 and -2 of hevamine (binding-subsite nomenclature according to [26]). In the structure of hevamine complexed with the allosamidin inhibitor [25], the main chain atoms of Gly^{81} ($L\beta_3\alpha_3$) and Ala^{224} ($L\beta_7\alpha_7$) make hydrogen-bonding contact with the allosamizoline moiety bound at subsite -1 while the main-chain NH group of Ile^{82} ($L\beta_3\alpha_3$) makes a direct hydrogen bond with the unit bound at subsite -2. In hevamine, the Cα distance between Gly^{81} and Ala^{224} (opposite side of -1 subsite) is 13.76 Å, whereas the corresponding distance in XIP-I is 17.88 Å between Tyr^{80} and Asp^{224}. Three aromatic residues (Trp^{255}, Tyr^{183} and Tyr^{6}) are present in the active centre of hevamine [25]. Trp^{255} and Tyr^{6} aromatic side chains stack against the hydrophobic face of the allosamizoline moiety of the allosamidin inhibitor. The hydroxy side chain of Tyr^{183} is within hydrogen-bonding distance of the -1 sugar residue of the substrate and contributes to catalysis [27]. These three aromatic residues are conserved in a structurally identical position in the structure of XIP-I; they correspond to Trp^{256}, Tyr^{189} and Phe^{11}. In Figure 2(B) the residues contributing to the binding of the ligand in the active-site cleft of hevamine from subsite -4 to subsite -2 (green) are superimposed with the corresponding residues in the groove region of XIP-I (blue). Hydrogen-bonding contacts were identified in the complex formed between hevamine and *N*,*N*′,*N*″-triacetylchitotriose (tri-NAG), a chitin fragment [28] involving main-chain atoms of residues Gly^{11}, Gly^{48}, Ala^{31}, Gly^{79}, and Ala^{47} as well as side chains of residues Gln^{9}, Asn^{45}, and Trp^{255}. In this part of the XIP-I depression, the side chains of the corresponding residues show similar conformations. Gln^{9} is replaced by Arg^{14}, which occupies the same space, has the same orientation and may participate in hydrogen and/or van der Waals contacts, as observed in the hevamine structure. Asn^{45} is replaced in similar conformation by Asp^{50}. The XIP-I structure contains three *cis*-peptides. A *cis*-proline, Pro^{167}, is present in the loop $L\beta_5\alpha_5$. Two other *cis*-peptides are located between Ser^{36} and Phe^{37} and between Trp^{256} and Asp^{257}. Phe^{37} and Trp^{256} emerge from strand $\beta2$ and from the end of strand $\beta8$ respectively and protrude into the heart of the groove on the

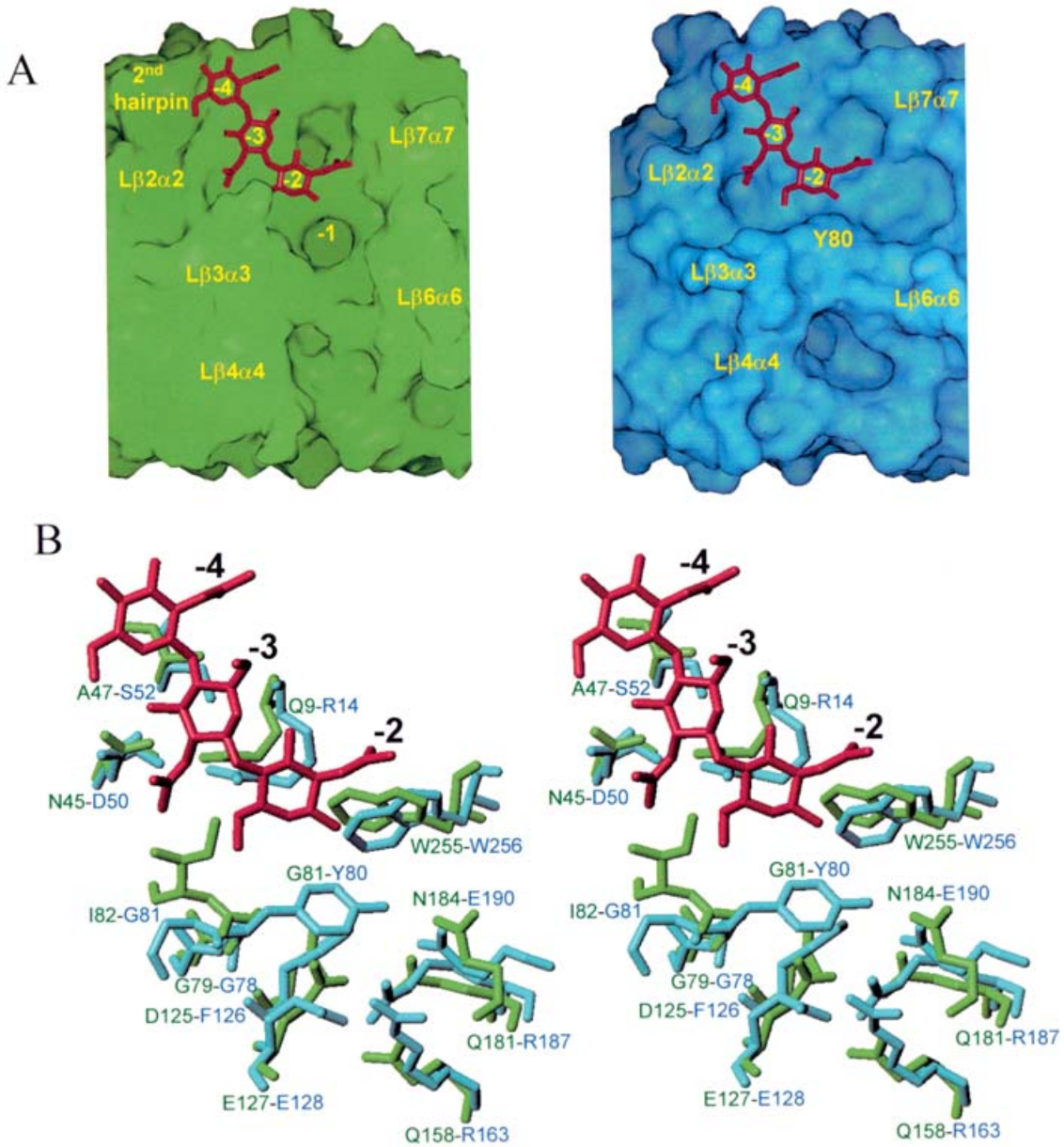

Figure 2 Comparison between the cleft structures in hevamine and XIP-I

(**A**) Surface representations showing the substrate-binding cleft of hevamine (green surface) with bound tri-NAG ligand (red) and the corresponding depression in XIP-I (blue surface). The upper part of the XIP-I depression resembles that of hevamine and might accommodate a sugar ligand. Residue Tyr^{80} creates a disruption in the cleft. This figure was prepared with SPOCK [30]. (**B**) The residues contributing to the binding of the ligand in hevamine (green) were superimposed on the corresponding residues in XIP-I (blue). The orientation and the colouring are the same as in (**A**), with hevamine residues displayed in green and XIP-I residues in blue. This view was generated with TURBO-FRODO [22].

top of the β-barrel which forms the rigid central part of the XIP-I molecule. Together with Phe^{126}, Phe^{11} and Tyr^{80} they form a cluster of aromatic residues. Two non-proline *cis*-peptide bonds are also observed in corresponding positions in the structures of hevamine (active-site region), concanavalin B and narbonin [10–12].

The long loop ($L\alpha_4\beta_5$) including residues 148–153 (Figure 1B) is characterized by the highest temperature factors of the molecule. Both the thermal parameters and the nature of the sequence (Ile-Arg-Gly-Gly-Pro-Gly) indicate high flexibility, suggesting that this loop region may play an important role in the inhibitor function. In the structures of hevamine, concanavalin B and narbonin, the corresponding loops are significantly shorter and are not structurally equivalent (see structural alignment in Figure 3).

Structural similarity with other family-18 GHs

Many aspects of the xylanase inhibitor structure are very similar to those found in hevamine [10]; indeed, the root-mean-square (r.m.s.) differences in 239 C^{α} positions after optimal superposition of the $(\beta/\alpha)_8$ molecule were 1.15 Å (program TURBO-FRODO; [22]). The structure of XIP-I is also similar to that of the two plant proteins, concanavalin B from *Canavalia ensiformis* [11], and, to a lesser extent, narbonin from *Vicia narbonensis* [12], both of which belong to GH family 18, but have no known enzymic activity. These proteins all show the $(\beta/\alpha)_8$ barrel fold and the two family-18 consensus regions, corresponding to the third and fourth barrel strands, are located in similar positions (see the

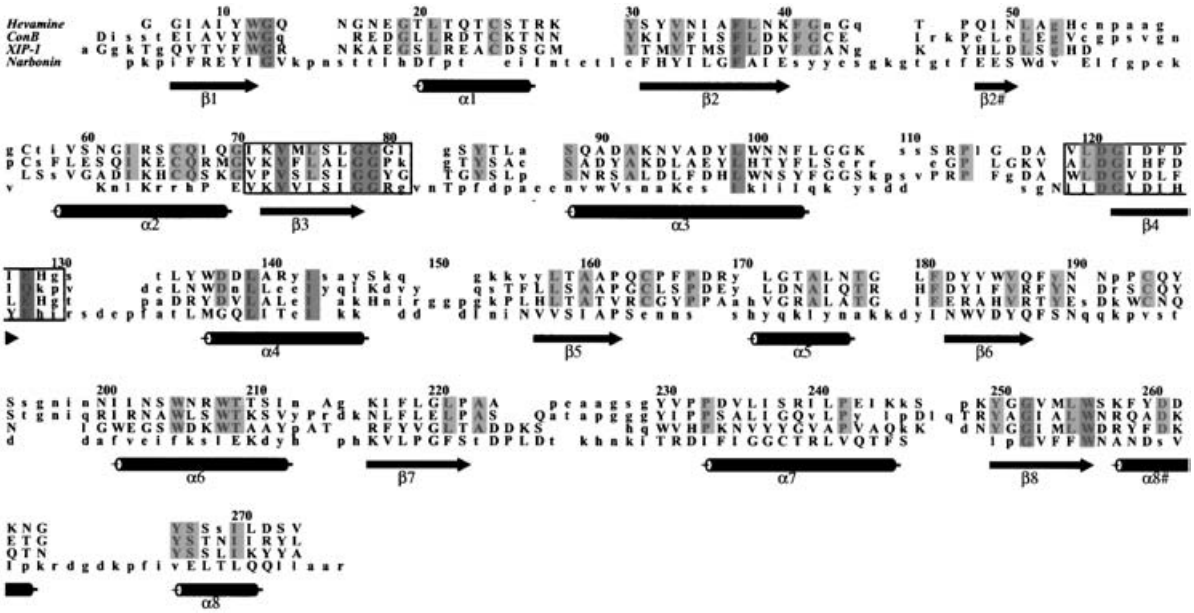

Figure 3 Sequence alignment based on structure superposition

Hevamine, concanavalin B and narbonin structures were superimposed on to the XIP-I structure using TURBO-FRODO [22]. The residues in which the C^{α} atoms were less than 2 Å apart were taken to be structurally equivalent and are shown in upper-case letters. Secondary-structure elements of XIP-I are numbered as in Figure 1(A). The conserved residues within the four sequences are coloured grey (light grey for the first three sequences). The two consensus regions are boxed. The position corresponding to the active residue in hevamine is shown in black. This Figure was constructed using ALSCRIPT [31].

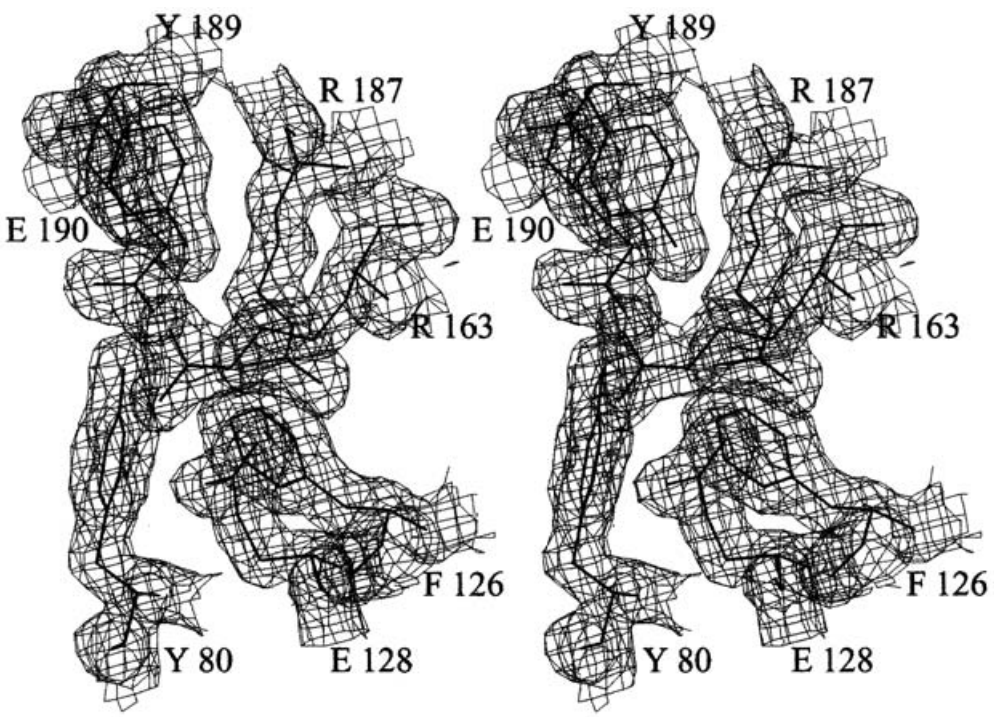

Figure 4 Glutamic acid residue environment in XIP-I

The Figure shows an electron-density map, in the XIP-I structure, for residues present in the area of the hevamine subsite −1. The density is from a $2F_o-F_c$ map, contoured at 1 σ. The two arginine residues interacting with Glu^{128} and the tyrosine residue protruding in front of this residue and hydrogen-bonded to Glu^{190} are shown.

boxed regions in Figure 3). In addition, hevamine, concanavalin B and narbonin display particular features typical of this family [10,11]: (i) the presence of an extended loop ($L\beta_2\alpha_2$) containing one or two antiparallel β-hairpins and (ii) the presence of non-proline *cis*-peptide bonds. These two typical features are also present in the structure of XIP-I. The unusual geometry of the *cis*-peptide bond occurs in structurally identical positions in hevamine (Ala^{31}–Phe^{32}; Trp^{255}–Ser^{256}) and in XIP-I (Ser^{36}–Phe^{37};

Trp^{256}–Asp^{257}). In the XIP-I L$\beta_2\alpha_2$ loop, only the first hairpin excursion following strand β2 is present. The following hairpin, closed by a disulphide bridge in the structures of hevamine (Cys^{50}–Cys^{57}) and concanavalin B (Cys^{54}–Cys^{62}), is replaced in the XIP-I structure by a short segment (see sequence alignments in Figure 3).

Lack of chitinase activity of XIP-I

The enzymes of the GH family 18 showing chitinase activity have a conserved aspartic acid and a catalytic glutamic acid residue in the active site, corresponding to Asp^{125} and Glu^{127} in hevamine. However, several proteins of this family are devoid of chitinase or known enzymic activity. In the structures of concanavalin B and narbonin, Asp^{125} and Glu^{127} are replaced by Asp^{129} and Gln^{131} and by His^{130} and Glu^{132} respectively [11,12], which mostly account for the lack of chitinase activity reported for these proteins. In XIP-I, the glutamic acid residue is present in an equivalent position (Glu^{128}), but its side chain is fully engaged in salt bridges with two neighbouring arginine residues, namely Arg^{187} and Arg^{163} (Figure 2B and Figure 4). A similar interaction was also observed in narbonin [12]. The glutamic acid residue Glu^{132} (narbonin numbering), present in an equivalent position to the catalytic residue in hevamine, was involved in a salt bridge with Arg^{87}; it has been suggested that this salt bridge prevents narbonin from acting as a chitinase, despite the presence of the catalytic residue [11,12]. Furthermore, the position equivalent to residue Asp^{125} in hevamine, which has been proposed to stabilize the positively charged oxazoline reaction intermediate [10], is occupied by Phe^{126} in XIP-I. The mutation of Asp^{125} to alanine in hevamine led to a mutant with approx. 2 % residual activity [27]. In narbonin, Asp^{125} is also replaced by a bulky residue, His^{130} [12].

The most striking disruption of the cleft in XIP-I is caused by the presence of the side chain of Tyr^{80}, which replaces Gly^{81} (L$\beta_3\alpha_3$) in hevamine. Located at subsite -1 of hevamine, Gly^{81} participates in the hydrogen-bonding network with the ligand [25,28]. In the structure of XIP-I, the side chain of Tyr^{80} (L$\beta_3\alpha_3$) protrudes into the cleft (Figure 2B and Figure 4) and forms a strong hydrogen bond with the side chain of Glu^{190} (L$\beta_6\alpha_6$), extending from the opposite side of the cleft. Both residues, located at opposite sides of the cleft, thus form a shield in front of residue Glu^{128}, resulting in complete obstruction of subsite -1 and preventing access to the catalytic residue. Here again it is worth noting that a similar structural arrangement was observed in narbonin, where Arg^{87} (L$\beta_3\alpha_3$), equivalent to Gly^{81} in hevamine, forms a salt bridge with Asp^{231} (L$\beta_7\alpha_7$), located on the opposite side of the cleft, resulting in the complete obstruction of subsite -1.

CONCLUSION

XIP-I is a new member of the family 18 GHs having a $(\beta/\alpha)_8$-barrel topology and a structure similar to that of hevamine, concanavalin B and narbonin. The lack of chitinase activity of XIP-I may be explained (i) by the presence of Tyr^{80} that fills subsite -1, where the reaction intermediate is formed, (ii) by differences in the loops (L$\beta_7\alpha_7$ and L$\beta_3\alpha_3$) that form the wall of the substrate-binding cleft in hevamine and (iii) by the absence of one of the two essential carboxylate groups. Although the catalytic glutamate residue is conserved in the sequence, its environment is different. Important residues involved in direct hydrogen bonds with the substrate-sugar unit bound at subsite -1 of hevamine, such as Asp^{125}, Gly^{81}, Ala^{224} and Glu^{127} are not conserved and/or are found in very different situations; only Tyr^{183} (Tyr^{189} in XIP-I) is conserved in structurally identical position in the structure of XIP-I. Moreover, the XIP-I crystal structure will provide a valuable tool for further understanding the specificity of the inhibition towards family-10 and family-11 endoxylanases.

This work was funded by Centre National de la Recherche Scientifique (CNRS) (France) and the European Union Framework V (GEMINI QLK1-2000-00811). We thank Dr A. Gruez, Dr S. Spinelli and J. Allouch (Architecture et Fonction des Macromolecules Biologiques, Centre National de la Recherche Scientifique, Marseille, France) for assistance in the synchrotron data collection. We thank Dr Bernard Henrissat (Architecture et Fonction des Macromolecules Biologiques, Centre National de la Recherche Scientifique, Marseille, France) for useful discussions and critical reading of the manuscript before its submission.

REFERENCES

1 McLauchlan, W. R., Garcia-Conesa, M. T., Williamson, G., Roza, M., Ravestein, P. and Maat, J. (1999) A novel class of protein from wheat which inhibits xylanases. Biochem J. **338**, 441–446
2 Debyser, W., Peumans, W. J., van Damme, E. J. M. and Delcour, J. A. (1999) *Triticum aestivum* xylanase inhibitor (TAXI), a new class of enzyme inhibitor affecting bread making performance. J. Cereal Sci. **30**, 39–43
3 Coutinho, P. M. and Henrissat, B. (1999) Carbohydrate-active enzymes: an integrated database approach. In Recent Advances in Carbohydrate Bioengineering (Gilbert, H. J., Davies, G. J., Henrissat, B. and Svensson, B., eds.), pp. 3–12, The Royal Society of Chemistry, Cambridge
4 White, A., Withers, S. G., Gilkes, N. R. and Rose, D. R. (1994) Crystal structure of the catalytic domain of the β-1,4-glycanase cex from *Cellulomonas fimi*. Biochemistry **33**, 12546–12552
5 Campbell, R., Rose, D., Wakarchuk, W., To, R., Sung, W. and Yaguchi, M. (1993) A comparison of the structures of the 20 kDa xylanases from *Trichoderma harzianum* and *Bacillus circulans*. In Proceedings of the Second TRICEL Symposium on *Trichoderma reesei* Cellulases and other Hydrolases, Espoo, Finland (Suouminen, P. and Reinikainen, T., eds.), pp. 63–72, Foundation for Biotechnological and Industrial Fermentation Research, Helsinki
6 Gebruers, K., Debyser, W., Goesaert, H., Proost, P., Van Damme, J. and Delcour, J. A. (2001) *Triticum aestivum* L. endoxylanase inhibitor (TAXI) consists of two inhibitors, TAXI I and TAXI II, with different specificities. Biochem. J. **353**, 239–244
7 Flatman, R., McLauchlan, W. R., Juge, N., Furniss, C., Berrin, J. G., Hughes, R. K., Manzanares, P., Ladbury, J. E., O'Brien, R. and Williamson, G. (2002) Interactions defining the specificity between fungal xylanases and the xylanase-inhibiting protein XIP-I from wheat. Biochem. J. **365** 773–781
8 Furniss, C. S. M., Belshaw, N. J., Alcocer, M. J., Williamson, G., Elliott, G. O., Gebruers, K., Haigh, N. P., Fish, N. M. and Kroon, P. A. (2002) A family 11 xylanase from *Penicillium funiculosum* is strongly inhibited by three wheat xylanase inhibitors. Biochim. Biophys. Acta **1598**, 24–29
9 Elliott, G. O., Hughes, R. K., Juge, N., Kroon, P. A. and Williamson, G. (2002) Functional identification of the cDNA coding for a wheat endo-1,4-β-D-xylanase inhibitor. FEBS Lett. **519**, 66–70
10 Terwisscha van Scheltinga, A. C., Hennig, M. and Dijkstra, B. W. (1996) The 1.8 Å resolution structure of hevamine, a plant chitinase/lysozyme, and analysis of the conserved sequence and structure motifs of glycosyl hydrolase family 18. J. Mol. Biol. **262**, 243–57
11 Hennig, M., Jansonius, J. N., Terwisscha van Scheltinga, A. C., Dijkstra, B. W. and Schlesier, B. (1995) Crystal structure of concanavalin B at 1.65 Å resolution. An "inactivated" chitinase from seeds of *Canavalia ensiformis*. J. Mol. Biol. **254**, 237–46
12 Hennig, M., Pfeffer-Hennig, S., Dauter, Z. and Wilson, K. (1995) Crystal structure of narbonin at 1.8 Å resolution. Acta Crystallogr. D Biol. Crystallogr. **51**, 177–189
13 Bokma, E., Spiering, M., Chow, K. S., Mulder, P., Subroto, T. and Beitema, J. J. (2001) Determination of cDNA and genomic DNA sequences of hevamine, a chitinase from the rubber tree *Hevea brasiliensis*. Plant Physiol. Biochem. **39**, 367–376
14 Schlesier, B., Nong, V. H., Horstmann, C. and Hennig, M. (1995) Sequence analysis of concanavalin B from *Canavalia ensiformis* reveals homology to chitinases. J. Plant Physiol. **147**, 665–674
15 Nong, V. H., Schlesier, B., Bassuner, R., Repik, A., Horstmann, C. and Muntz, K. (1995) Narbonin, a novel 2 S protein from *Vicia narbonensis* L. seeds: cDNA, gene structure and developmentally regulated formation. Plant Mol. Biol. **28**, 61–72
16 Tata, S. J., Beintema, J. J. and Balabaskaram, S. (1983) The lysozyme of *Hevea brasiliensis* latex: isolation, purification, enzyme kinetics and a partial amino-acid sequence. J. Rubber Res. Inst. Malaysia **31**, 35–48

17 Tahir, T. A., Berrin, J. G., Flatman, R., Roussel, A., Roepstorff, P., Williamson, G. and Juge, N. (2002) Specific characterization of substrate and inhibitor binding sites of a glycosyl hydrolase family 11 xylanase from *Aspergillus niger*. J. Biol. Chem. **277**, 44035–44043
18 Torronen, A., Harkki, A. and Rouvinen, J. (1994) Three-dimensional structure of endo-1,4-β-xylanase II from *Trichoderma reesei*: two conformational states in the active site. EMBO J. **13**, 2493–2501
19 Otwinowski, Z. and Minor, W. (1997) Processing of X-ray diffraction data collected in oscillation mode. Methods Enzymol. **276**, 307–326
20 Navaza, J. (1994) AMoRe: an automated package for molecular replacement. Acta Crystallogr. A **50**, 157–163
21 Brunger, A. T., Adams, P. D., Clore, G. M., DeLano, W. L., Gros, P., Grosse-Kunstleve, R. W., Jiang, J. S., Kuszewski, J., Nilges, M., Pannu, N. S. et al. (1998) Crystallography and NMR system: A new software suite for macromolecular structure determination. Acta Crystallogr. D Biol. Crystallogr. **54**, 905–921
22 Roussel, A. and Cambillau, C. (1991) Silicon Graphics Geometry Patterns Directory, pp. 86, Silicon Graphics, Mountain View, CA
23 Ramachandran, G. N. and Sasisekharan, V. (1968) Conformation of polypeptides and proteins. Adv. Protein Chem. **23**, 283–438
24 Laskowski, R. A., Moss, D. S. and Thornton, J. M. (1993) Main-chain bond lengths and bond angles in protein structures. J. Mol. Biol. **231**, 1049–1067
25 Terwisscha van Scheltinga, A. C., Armand, S., Kalk, K. H., Isogai, A., Henrissat, B. and Dijkstra, B. W. (1995) Stereochemistry of chitin hydrolysis by a plant chitinase/lysozyme and X-ray structure of a complex with allosamidin: evidence for substrate assisted catalysis. Biochemistry **34**, 15619–15623
26 Davies, G. J., Wilson, K. S. and Henrissat, B. (1997) Nomenclature for sugar-binding subsites in glycosyl hydrolases. Biochem. J. **321**, 557–559
27 Bokma, E., Rozeboom, H. J., Sibbald, M., Dijkstra, B. W. and Beintena, J. J. (2002) Expression and characterization of active site mutants of hevamine, a chitinase from the rubber tree *Hevea brasiliensis*. Eur. J. Biochem. **269**, 893–901
28 Terwisscha van Scheltinga, A. C., Kalk, K. H., Beintema, J. J. and Dijkstra, B. W. (1994) Crystal structures of hevamine, a plant defence protein with chitinase and lysozyme activity, and its complex with an inhibitor. Structure **2**, 1181–1189
29 Kraulis, P. J. (1991) MOLSCRIPT: a program to produce both detailed and schematic plots of protein structures. J. Appl. Crystallogr. **24**, 946–950
30 Christopher, J. A. (1998) SPOCK: The Structural Properties Observation and Calculation Kit Program Manual, Center for Macromolecular Design and Texas A&M University, College Station, TX
31 Barton, G. J. (1993) ALSCRIPT: a tool to format multiple sequence alignments. Protein Eng. **6**, 37–40

Received 19 November 2002/27 February 2003; accepted 5 March 2003
Published as BJ Immediate Publication 5 March 2003, DOI 10.1042/BJ20021802